phys. stat. sol. (a) **197**, No. 3, 637–647 (2003) / **DOI** 10.1002/pssa.200303111

A solid state theoretical approach to the optical properties of photonic crystals

Kurt Busch[*,1], **Meikel Frank**[1], **Antonio Garcia-Martin**[1,2], **Daniel Hermann**[1], **Sergei F. Mingaleev**[1,3], **Matthias Schillinger**[1], and **Lasha Tkeshelashvili**[1]

[1] Institut für Theorie der Kondensierten Materie, Universität Karlsruhe, 76128 Karlsruhe, Germany
[2] Instituto de Microelectronica de Madrid, Consejo Superior de Investigaciones Cientificas, Issac Newton, 8 (PTM), 28760 Tres Cantos, Madrid, Spain
[3] Bogolyubov Institute for Theoretical Physics, 03143 Kiev, Ukraine

Received 15 October 2002, revised 4 April 2003, accepted 7 April 2003
Published online 20 June 2003

PACS 41.20.Jb, 42.65.–k, 42.70.Qs

We outline a theoretical framework that allows qualitative as well as quantitative analysis of the optical properties of Photonic Crystals (PCs) and which is derived from solid state theoretical concepts. Starting from photonic bandstructure computations which allow us to obtain dispersion relations and associated Bloch functions, we show how related physical quantities such as densities of states and group velocities can be calculated. In addition, defect structures embedded in PCs can be efficiently treated with the help of photonic Wannier functions that are derived from photonic Bloch functions by means of a lattice Fourier transform. Nonlinear PCs may be investigated by an appropriate multi-scale analysis utilizing Bloch functions as carrier waves together with an adaptation of $\boldsymbol{k}\cdot\boldsymbol{p}$-perturbation theory. This leads to a natural generalization of the slowly varying envelope approximation to the case of nonlinear wave propagation in PCs.

1 Introduction

Progress in Photonics is intimately related to the development of optical materials with tailor made properties. Photonic Crystals (PCs) carry this principle to a new level of sophistication in the sense that the photonic dispersion relation and associated mode structure may be tailored to almost any need through a judicious design of these two-dimensional (2D) or three-dimensional (3D) periodic dielectric arrays. In particular, the choice of material composition, lattice periodicity and symmetry as well as the deliberate creation of defect structures embedded in PCs allows a degree of control over the properties of this novel class of optical materials that may eventually rival the flexibility in tailoring the properties of their electronic counterparts, the semiconducting materials.

The usefulness of PCs derives to a large extent from the fact that suitably engineered PCs may exhibit one or more photonic band gaps (PBGs) [1–3]. For instance, recent experiments have verified earlier theoretical predictions that 3D PCs such as the inverse opals [4, 5] exhibit frequency ranges over which ordinary linear propagation is forbidden irrespective of direction. The existence of these complete PBGs allows complete control over the radiative dynamics of active material embedded in PCs such as the inhibition of spontaneous emission for atomic transition frequencies deep in the PBG

[*] Corresponding author: e-mail: kurt@tkm.physik.uni-karlsruhe.de

 0031-8965/03/19706-0637 $ 17.50+.50/0

[1] and leads to strongly non-Markovian effects such as fractional localization of the atomic population for atomic transition frequencies in close proximity to a complete PBG [6, 7].

For a number of applications such as guided light in planar waveguide structures and most nonlinear wave mixing experiments it is sufficient to obtain control over the propagation of light within the corresponding plane of propagation. As a consequence, 2D PCs and their 2D PBGs come into play. For such structures, advanced planar micro-structuring techniques borrowed from semiconductor technology can greatly simplify the fabrication process. Depending on the desired aspect ratio of sample depth (vertical direction) to lattice constant (transverse direction), high-quality 2D PCs can be manufactured through plasma etching and lithography techniques [8–10] (aspect ratios up to 5 : 1) or through photo-electrochemically growing ordered macro-pores into silicon wafers [11, 12] (aspect ratios up to 200 : 1). In the linear regime, PBGs in 2D PCs offer novel passive optical guiding characteristics through the engineering of defects such as microcavities and waveguides and their combination into functional elements such as wavelength add-drop filters [13, 14]. Similarly, the incorporation of nonlinear materials into 2D PBG structures creates the possibility for novel solitary wave propagation for frequencies inside the PBG, where ordinary linear propagation is forbidden. In the case of lattice-periodic Kerr-nonlinearities the threshold intensities and symmetries of these solitary waves depend on the direction of propagation [15–17], whereas in the case of nonlinear waveguiding structures embedded in a 2D PBG material the propagation characteristics strongly depend on the nature of the waveguides [18].

As compared to the numerous applications of 2D and 3D PBGs, wave propagation in linear and nonlinear PCs for frequencies inside photonic bands has received far less attention. However, the recent discovery of superrefractive phenomena such as the superprism effect [19] that are based on the highly anisotropic nature of iso-frequency surfaces in the photonic bandstructure suggest a number of potential applications specifically in optical telecommunication technology [20]. Therefore, they provide a valuable addition to the rich physics of wave propagation in PCs [21, 22]. Similarly, in the context of nonlinear optical phenomena it is the tailoring of photonic dispersion relations and mode structures through judiciously designed PCs that allows to explore regimes for parameters such as group velocity, group velocity dispersion (GVD) and effective nonlinearities that hitherto have been virtually inaccessible. For instance, the existence of flat bands that are characteristic for 2D and 3D PCs and the associated low group velocities may greatly enhance frequency conversion effects [23] and may lead to improved designs for distributed-feedback (DFB) laser systems [23–25].

Any experimental exploration as well as technological exploitation of the huge parameter space provided by PCs has to be accompanied by a quantitative theoretical analysis in order to identify the most interesting cases and help to interpret the data as well as to find stable designs for successfully operating devices. In this manuscript, we provide an outline for a theoretical framework that allows to qualitatively as well as quantitatively determine the optical properties of PCs that is based on solid state theoretical concepts: Photonic bandstructure computations allow us to obtain dispersion relations and associated mode structures (Bloch functions). Related physical quantities such as densities of states and group velocities can be calculated with little additional work (Section 2). In addition, we show how defect structures can be efficiently treated with the help of photonic Wannier functions (Section 3). Finally, nonlinear PCs may be investigated by an appropriate multi-scale analysis that utilizes Bloch functions. This leads to a generalization of the well-known sowly varying envelope approximation (Section 4).

2 Photonic bandstructure computation

The goal of photonic bandstructure computation is the solution of the wave equation for the perfect PC, i.e., for a strictly periodic array of dielectric material. The resulting dispersion relation and associated mode structure may then be further processed to derive related physical quantities such as densities of states and group velocities. For simplicity of presentation we consider in the remainder of the manuscript only 2D PCs in the TM-polarized case. However, we want to emphasize that analogous considerations apply to the case of TE-polarized radiation in 2D PCs as well as to electromagnetic wave propagation in 3D PCs and will give references where appropriate.

For TM-polarized radiation in 2D PCs the wave equation reduces to a single scalar equation for the z-component $E(\boldsymbol{r})$of the electric field

$$\frac{1}{\epsilon_{\mathrm{p}}(\boldsymbol{r})}\,(\partial_x^2+\partial_y^2)\,E(\boldsymbol{r})+\frac{\omega^2}{c^2}\,E(\boldsymbol{r})=0\,. \tag{1}$$

Here c denotes the vacuum speed of light and $\boldsymbol{r}=(x,y)$ denotes a two-dimensional position vector. The dielectric constant $\epsilon_{\mathrm{p}}(\boldsymbol{r})\equiv\epsilon_{\mathrm{p}}(\boldsymbol{r}+\boldsymbol{R})$ contains all the structural information of the PC and is periodic with respect to the set $\mathcal{R}=\{n_1\boldsymbol{a}_1+n_2\boldsymbol{a}_2;(n_1,n_2)\in\mathcal{Z}^2\}$ of lattice vectors $\boldsymbol{R}$ generated by the primitive translations $\boldsymbol{a}_i, i=1,2$ which serve as a basis for the underlying PC lattice. Eq. (1) represents a differential equation with periodic coefficients and, therefore, its solutions obey the Bloch-Floquet theorem: Due to the discrete translational symmetry of the lattice, the wave vector $\boldsymbol{k}$ labeling the solutions may be restricted to lie in the first Brillouin zone (BZ) of the reciprocal lattice. As a consequence, the dispersion relation $\omega(\boldsymbol{k})$ in the infinitely extended momentum space is folded back onto the first BZ, introducing a discrete band index n. The eigenmodes corresponding to the eigenfrequency $\omega_n(\boldsymbol{k})$ exhibit Bloch-Floquet form

$$E_{n\boldsymbol{k}}(\boldsymbol{r})=\mathrm{e}^{i\boldsymbol{k}\boldsymbol{r}}\,u_{n\boldsymbol{k}}(\boldsymbol{r})\,, \tag{2}$$

where $u_{n\boldsymbol{k}}(\boldsymbol{r}+\boldsymbol{R})=u_{n\boldsymbol{k}}(\boldsymbol{r})$ is a lattice periodic function. A straightforward way of solving Eqs. (1) and (2) is to expand all the periodic functions into a Fourier series over the reciprocal lattice $\mathcal{G}$

$$\frac{1}{\epsilon_{\mathrm{p}}(\boldsymbol{r})}=\sum_{\boldsymbol{G}}\eta_{\boldsymbol{G}}\,\mathrm{e}^{i\boldsymbol{G}\cdot\boldsymbol{r}}\,,\qquad E_{\boldsymbol{k}}(\boldsymbol{r})=\sum_{\boldsymbol{G}}a_{\boldsymbol{G}}^{\boldsymbol{k}}\,\mathrm{e}^{i(\boldsymbol{k}+\boldsymbol{G})\cdot\boldsymbol{r}}\,. \tag{3}$$

The Fourier coefficients $\eta_{\boldsymbol{G}}$ are given by

$$\eta_{\boldsymbol{G}}=\frac{1}{V_{\mathrm{WSC}}}\int\limits_{\mathrm{WSC}}d^2\boldsymbol{r}\;\frac{1}{\epsilon_{\mathrm{p}}(\boldsymbol{r})}\,\mathrm{e}^{-i\boldsymbol{G}\cdot\boldsymbol{r}}\,, \tag{4}$$

where we have designated the volume of the Wigner–Seitz cell (WSC) by V_{WSC}. Inserting this expansion into Eq. (1) and defining the coefficients $b_{\boldsymbol{G}}^{\boldsymbol{k}}\equiv|\boldsymbol{k}+\boldsymbol{G}|\,a_{\boldsymbol{G}}^{\boldsymbol{k}}$, transforms the differential equation into an infinite matrix eigenvalue problem

$$\sum_{\boldsymbol{G}'}|\boldsymbol{k}+\boldsymbol{G}|\,|\boldsymbol{k}+\boldsymbol{G}'|\;\eta_{\boldsymbol{G}-\boldsymbol{G}'}b_{\boldsymbol{G}'}^{\boldsymbol{k}}=\frac{\omega_{\boldsymbol{k}}^2}{c^2}\,b_{\boldsymbol{G}}^{\boldsymbol{k}}\,, \tag{5}$$

which must be suitably truncated to become accessible to an approximate numerical solution. Owing to this simplicity and flexibility in handling practically any geometry of the unit cell through Eq. (4), this plane wave method (PWM) has become the work horse for most investigations of photonic bandstructures. Further details of the PWM for 2D TE and 3D isotropic systems can be found, for instance, in [26] and for anisotropic 3D systems in [27].

In Fig. 1b, we show the bandstructure for TM-polarized radiation in a 2D PC consisting of a square lattice (lattice constant a) of cylindrical dielectric rods (radius $R_{\mathrm{rod}}=0.18a$ and dielectric constant $\varepsilon_{\mathrm{rod}}=11.56$ (silicon)) in air. This structure exhibits two complete bandgaps. The larger, fundamental bandgap (38% of the midgap frequency) extends between $\omega=0.302\times2\pi c/a$ to $\omega=0.443\times2\pi c/a$ and the smaller, higher order bandgap (3% of the midgap frequency) extends from $\omega=0.738\times2\pi c/a$ to $\omega=0.763\times2\pi c/a$. In Section 3, we will use this particular PC in order to illustrate the Wannier function approach to the accurate and efficient calculation of defect structures embedded in PCs. Furthermore, we want to point out that the bands 2, 3, and 4 exhibit wildly different group velocities. For instance, while the third band displays very low and almost constant group velocities for all wave vectors in Γ-X and Γ-M direction, the first and fourth bands exhibit variations between zero and intermediate values of group velocities for the same set of wave vectors. This behavior is generic to 2D and 3D PCs and does not occur in 1D PCs.

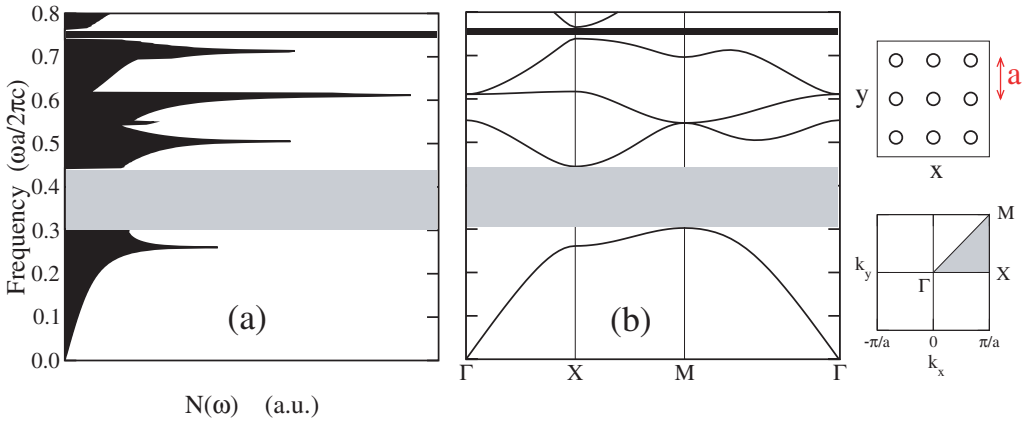

Fig. 1 Density of States a) and photonic band structure b) for TM-polarized radiation in a square lattice (lattice constant a) of cylindrical dielectric rods (radius $R_{\text{rod}} = 0.18a$ and $\varepsilon_{\text{rod}} = 11.56$ (silicon)) in air. This PC exhibits a large fundamental gap extending from $\omega = 0.302 \times 2\pi c/a$ to $\omega = 0.443 \times 2\pi c/a$. A higher order band gap extends from $\omega = 0.738 \times 2\pi c/a$ to $\omega = 0.763 \times 2\pi c/a$.

2.1 Density of states

The photonic dispersion relation $\omega_n(\boldsymbol{k})$ gives rise to a photonic Density of States (DOS), which plays a fundamental role in the understanding of the properties of a PC [7]. The photonic DOS $N(\omega)$ is defined by "counting" all allowed states with a given frequency ω, i.e., by the sum of all bands and the integral over the first BZ of a Dirac-δ function

$$N(\omega) = \sum_n \int_{BZ} d^2k \delta(\omega - \omega_n(\boldsymbol{k}))\,. \tag{6}$$

The DOS for our model system is depicted in Fig. 1a which displays the photonic band gaps as regions of vanishing DOS. Characteristic for 2D systems is the linear behavior for small frequencies as well as the logarithmic singularities, the so-called van Hove singularities, associated with vanishing group velocities for certain frequencies inside the bands. However, for applications to quantum optical experiments in photonic crystals it is necessary to investigate not only the (overall) availability of modes with frequency ω but also the local coupling between an excited atom that can emit a photon with frequency ω and the electromagnetic environment provided by the photonic crystal at the location of the atom. Consequently it is the overlap matrix element of the atomic dipole moment to the photons in this mode that is determining quantum optical properties such as decay rates etc. [7]. This may be combined into the local DOS (LDOS), $N(\boldsymbol{r}, \omega)$, defined as

$$N(\boldsymbol{r}, \omega) = \sum_n \int_{BZ} d^2k |E_{n\boldsymbol{k}}(\boldsymbol{r})|^2\, \delta(\omega - \omega_n(\boldsymbol{k}))\,. \tag{7}$$

For an actual calculation, the integrals in Eqs. (6) and (7) must be suitably discretized and one may again revert to the methods of electronic band structure calculations (see Ref. [26]).

2.2 Group velocity and group velocity dispersion

In order to understand pulse propagation in linear and nonlinear PCs, it is necessary to obtain group velocities and group velocity dispersion (GVD) from the photonic bandstructure. In principle, this can be done through a simple numerical differentiation of the bandstructure, but in particular for the GVD this becomes computationally involved and great care must be exercised in order to avoid numerical instabilities. Therefore, we want to demonstrate how to obtain group velocities and group velocity dispersion through an adaptation of the so-called $\boldsymbol{k} \cdot \boldsymbol{p}$-perturbation theory ($kp$-PT) of electronic band

structure theory. This approach has been applied to systems of arbitrary dimension [28–30] and will be particularly useful for the investigation of nonlinear effects in PC as discussed in Section 4.

Using the Bloch–Floquet theorem Eq. (2), we may rewrite the wave Eq. (1) into an equation of motion for the lattice-periodic functions $u_{\boldsymbol{k}}(\boldsymbol{r})$

$$(\Delta + 2i\,\nabla\cdot\boldsymbol{k} - \boldsymbol{k}^2)\,u_{\boldsymbol{k}}(\boldsymbol{r}) + \frac{\omega_{\boldsymbol{k}}^2}{c^2}\,\epsilon_{\mathrm{p}}(\boldsymbol{r})\,u_{\boldsymbol{k}}(\boldsymbol{r}) = 0\,. \tag{8}$$

The introduction of the operator $\hat{\boldsymbol{H}}(\boldsymbol{k}) = \Delta + 2i\nabla\cdot\boldsymbol{k} - \boldsymbol{k}^2$, where $\Delta = \partial_x^2 + \partial_y^2$, allows us to cast Eq. (8) for the lattice-periodic $u_{\boldsymbol{k}+\boldsymbol{q}}(\boldsymbol{r})$ for a nearby wave vector $\boldsymbol{k}+\boldsymbol{q}$ ($|\boldsymbol{q}| \ll \pi/a$) into the form

$$\hat{\boldsymbol{H}}(\boldsymbol{k})\,u_{\boldsymbol{k}+\boldsymbol{q}}(\boldsymbol{r}) - (2\boldsymbol{q}\cdot\boldsymbol{\Omega} + |\boldsymbol{q}|^2)\,u_{\boldsymbol{k}+\boldsymbol{q}}(\boldsymbol{r}) + \frac{\omega_{\boldsymbol{k}+\boldsymbol{q}}^2}{c^2}\,\epsilon(\boldsymbol{r})_{\mathrm{p}}\,u_{\boldsymbol{k}+\boldsymbol{q}}(\boldsymbol{r}) = 0\,. \tag{9}$$

Here, we have introduced $\hat{\boldsymbol{\Omega}} = -i(\nabla + i\boldsymbol{k})$. Together with the smallness of the wave vector $\boldsymbol{q}$ Eq. (9) suggests that we treat the second and third term on the l.h.s as a perturbation to the operator $\hat{\boldsymbol{H}}(\boldsymbol{k})$ with eigenfrequencies $\omega_{\boldsymbol{k}}$. The "perturbed" eigenfrequency $\omega_{\boldsymbol{k}+\boldsymbol{q}}$ can then be calculated from the knowledge of *all* the unperturbed eigenfrequencies $\omega_{\boldsymbol{k}}$ and Bloch functions $E_{\boldsymbol{k}}(\boldsymbol{r})$ at wave vector $\boldsymbol{k}$ which are readily available from photonic bandstructure calculations. Comparing the perturbation series with a Taylor-expansion of $\omega_{\boldsymbol{k}+\boldsymbol{q}}$ around $\boldsymbol{k}$

$$\omega_{\boldsymbol{k}+\boldsymbol{q}} = \omega_{\boldsymbol{k}} + (1\text{st order } kp\text{-PT}) + (2\text{nd order } kp\text{-PT})\ldots + = \omega_{\boldsymbol{k}} + \boldsymbol{q}\cdot\boldsymbol{v}_{\boldsymbol{k}} + \boldsymbol{q}\cdot M_{\boldsymbol{k}}\cdot\boldsymbol{q} + \ldots\,, \tag{10}$$

connects group velocities $\boldsymbol{v}_{\boldsymbol{k}} = \partial_{\boldsymbol{k}}\omega_{\boldsymbol{k}}$ and GVD tensor elements $M_{\boldsymbol{k}}^{ij} = \partial_{k_i}\partial_{k_j}\omega_{\boldsymbol{k}}$, $i = 1,2$ to expressions familiar from second order perturbation theory [28–30]. Using the notation

$$\int_{\mathrm{WSC}} \mathrm{d}^2 r\, E_{n\boldsymbol{k}}^*(\boldsymbol{r})\,\hat{\boldsymbol{O}}\,E_{m\boldsymbol{k}}(\boldsymbol{r}) = \langle n\boldsymbol{k}|\,\hat{\boldsymbol{O}}\,|m\boldsymbol{k}\rangle\,, \tag{11}$$

for the matrix elements of the operator $\hat{\boldsymbol{O}}$ between Bloch functions $E_{n\boldsymbol{k}}(\boldsymbol{r})$ and $E_{m\boldsymbol{k}}(\boldsymbol{r})$, we obtain for the group velocity $\boldsymbol{v}_{n\boldsymbol{k}}$

$$\boldsymbol{v}_{n\boldsymbol{k}} = \frac{c^2}{\omega_{n\boldsymbol{k}}}\,\langle n\boldsymbol{k}| - i\nabla_{\boldsymbol{r}}\,|n\boldsymbol{k}\rangle\,, \tag{12}$$

and for the GVD tensor $\mathcal{M}_{n\boldsymbol{k}}$

$$\begin{aligned}\boldsymbol{q}\cdot\mathcal{M}_{n\boldsymbol{k}}\cdot\boldsymbol{q} = {} & |\boldsymbol{q}|^2\,\frac{c^2}{2\omega_{n\boldsymbol{k}}}\langle n\boldsymbol{k}\,|\,n\boldsymbol{k}\rangle - \frac{1}{2\omega_{n\boldsymbol{k}}}\,(\boldsymbol{q}\cdot\boldsymbol{v}_{n\boldsymbol{k}})^2 \\ & + \frac{2c^4}{\omega_{n\boldsymbol{k}}}\sum_{m\neq n}\frac{\langle n\boldsymbol{k}| - i\boldsymbol{q}\cdot\nabla\,|m\boldsymbol{k}\rangle\,\langle m\boldsymbol{k}| - i\boldsymbol{q}\cdot\,\nabla|n\boldsymbol{k}\rangle}{\omega_{n\boldsymbol{k}}^2 - \omega_{m\boldsymbol{k}}^2}\,.\end{aligned} \tag{13}$$

Despite their complicated appearance, these expressions can be evaluated rather easily using standard PWM and allow very accurate, efficient and numerically stable results.

3 Defect structures in photonic crystals

In electronic micro-circuits, electrical currents are guided by thin metal wires where electrons are bound within the cross section of the wire by the so-called work function (confining potential) of the metal. As a result, electrical currents follow the path prescribed by the wire without escaping to the background. The situation is very different for optical waves. Although optical fibers guide light over long distances, microscopic fiber-circuits for light do not exist, because empty space is already an ideal conductor of light waves. The light in an optical fiber can easily escape into the background electromagnetic modes of empty space if the fiber is bent or distorted on a microscopic scale. PBGs in the bandstructure of PCs remove this problem by removing all the background electromagnetic modes over the relevant band of frequencies. As a consequence, light paths can be created inside a PBG material in the form of engineered waveguide channels. The PBG localizes the light and pre-

vents it from escaping the optical micro-circuit. To date, theoretical investigations of defect structures in PCs have almost exclusively been carried out using finite difference time domain (FDTD) methods [13, 14]. However, applying general purpose methodologies such as FDTD or finite element (FEM) methods to defect structures in PCs largely disregards information about the underlying PC structure which is readily available from photonic bandstructure computation.

A more natural description of localized defect modes in PCs consists in an expansion of the electromagnetic field into a set of localized basis functions which have encoded into them all the information of the underlying PC. Therefore, the most natural set of basis functions for the description of defect structures in PCs consists in the so-called photonic Wannier functions $W_{n\boldsymbol{R}}(\boldsymbol{r})$, which are formally defined through a lattice Fourier transform of the extended Bloch functions $E_{n\boldsymbol{k}}(\boldsymbol{r})$

$$W_{n\boldsymbol{R}}(\boldsymbol{r}) = \frac{V_{\mathrm{WSC}}}{(2\pi)^2} \int\limits_{\mathrm{BZ}} d^2\boldsymbol{k}\, \mathrm{e}^{-i\boldsymbol{k}\boldsymbol{R}}\, E_{n\boldsymbol{k}}(\boldsymbol{r})\,. \tag{14}$$

The above definition associates the photonic Wannier function $W_{n\boldsymbol{R}}(\boldsymbol{r})$ with the frequency range covered by band n and centers it around the corresponding lattice site $\boldsymbol{R}$. In addition, the completeness and orthogonality of the Bloch functions translates directly in corresponding properties of the photonic Wannier functions

$$\int\limits_{\mathrm{V}} d^2\boldsymbol{r} W^*_{n\boldsymbol{R}}(\boldsymbol{r})\, \varepsilon_{\mathrm{p}}(\boldsymbol{r})\, W_{n'\boldsymbol{R}'}(\boldsymbol{r}) = \delta_{nn'}\, \delta_{\boldsymbol{R}\boldsymbol{R}'}\,. \tag{15}$$

However, it is straightforward to show that for a group of N bands there exists for every wave vector $\boldsymbol{k}$ a free unitary transformation $U_{mn}(\boldsymbol{k})$ between the bands

$$E_{n\boldsymbol{k}}(\boldsymbol{r}) \rightarrow \sum_{m=1}^{N} U_{mn}(\boldsymbol{k})\, E_{m\boldsymbol{k}}(\boldsymbol{r})\,, \tag{16}$$

which leaves the orthogonality relation Eq. (15) unchanged. This indeterminacy of the Wannier function has a profound influence on their localization properties [31, 32]. The way out has been described by Marzari and Vanderbilt [33, 34]: An unique transformation $U_{mn}(\boldsymbol{k})$ can be found numerically by minimizing an appropriate spread functional. In turn, this leads to the construction of maximally localized Wannier functions through Eqs. (16) and (14). In view of the translational properties of the Wannier functions,

$$W_{n\boldsymbol{R}}(\boldsymbol{r}) = W_{n\boldsymbol{0}}(\boldsymbol{r} - \boldsymbol{R})\,, \tag{17}$$

this functional reads

$$\Omega = \sum_{n=1}^{N} \left[\langle n\boldsymbol{0}|\, r^2\, |n\boldsymbol{0}\rangle - \left(\langle n\boldsymbol{0}|\, \boldsymbol{r}\, |n\boldsymbol{0}\rangle\right)^2\right] = \mathrm{Min.}\,, \tag{18}$$

where the matrix element $\langle n\boldsymbol{R}|\, \hat{\boldsymbol{O}}\, |m\boldsymbol{S}\rangle$ of the operator $\hat{\boldsymbol{O}}$ between the Wannier functions $W_{n\boldsymbol{R}}(\boldsymbol{r})$ and $W_{m\boldsymbol{S}}(\boldsymbol{r})$ has been defined similar to Eq. (11). Clearly, the above considerations can equally well be applied to the construction of photonic Wannier functions for 2D TM [31, 32, 36], 2D TE [35] and 3D systems. The field distributions of the maximally localized Wannier functions belonging to the six lowest bands of our model system are depicted in Fig. 2. Their localization properties as well as the symmetries of the underlying PC structure are clearly visible.

The description of defect structures embedded in PCs starts with the corresponding wave equation in the frequency domain

$$\nabla^2 E(\boldsymbol{r}) + \left(\frac{\omega}{c}\right)^2 \left\{\varepsilon_p(\boldsymbol{r}) + \delta\varepsilon(\boldsymbol{r})\right\} E(\boldsymbol{r}) = 0\,. \tag{19}$$

Here, we have decomposed the dielectric function into the periodic part $\varepsilon_{\mathrm{p}}(\boldsymbol{r})$ and the contribution that describes the defect structures $\delta\varepsilon(\boldsymbol{r})$. Within the Wannier function approach, we expand the electro-

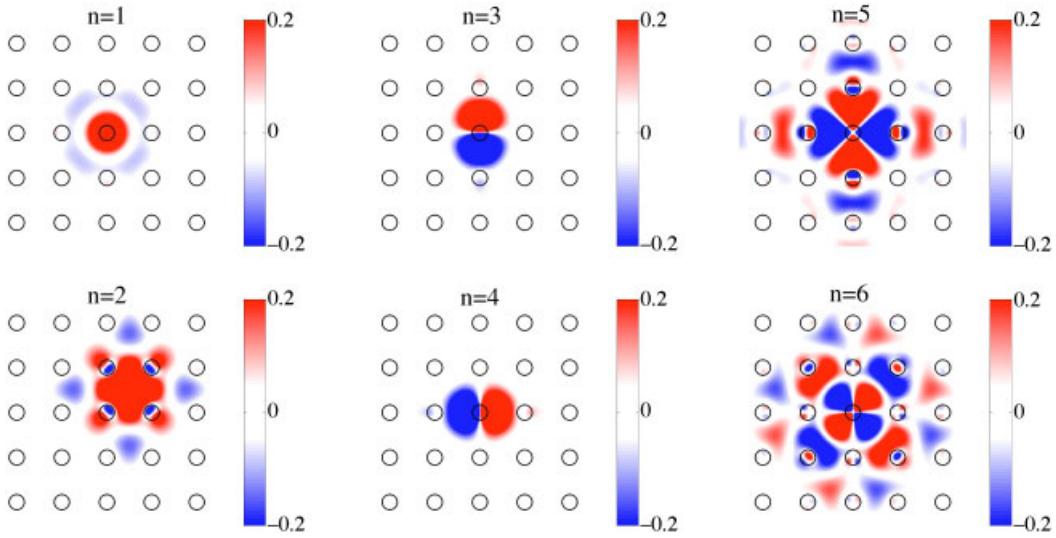

Fig. 2 Maximally localized photonic Wannier functions $W_{n\boldsymbol{0}}(\boldsymbol{r})$ for the first six bands obtained by minimizing the corresponding spread functional, Eq. (18). Note, that in contrast to the other bands, the Wannier center of the second band is located halfway between the cylinders. The parameters of the underlying PC are the same as those in Fig 1.

magnetic field according to

$$E(\boldsymbol{r}) = \sum_{n,\boldsymbol{R}} E_{n\boldsymbol{R}} W_{n\boldsymbol{R}}(\boldsymbol{r}) \,, \tag{20}$$

with unknown amplitudes $E_{n\boldsymbol{R}}$. Inserting this expansion into the wave Eq. (19) leads to the basic equation for lattice models describing defect structures embedded in PCs

$$\sum_{n',\boldsymbol{R}'} \{\delta_{nn'}\, \delta_{\boldsymbol{R}\boldsymbol{R}'} + D^{nn'}_{\boldsymbol{R}\boldsymbol{R}'}\}\, E_{n'\boldsymbol{R}'} = \left(\frac{c}{\omega}\right)^2 \sum_{n',\boldsymbol{R}'} A^{nn'}_{\boldsymbol{R}\boldsymbol{R}'} E_{n'\boldsymbol{R}'} \,. \tag{21}$$

The matrix $A^{nn'}_{\boldsymbol{R}\boldsymbol{R}'}$ depends only on the dispersion relation and Wannier functions of the underlying PC and is defined through

$$A^{nn'}_{\boldsymbol{R}\boldsymbol{R}'} = \frac{V_{\mathrm{WSC}}}{(2\pi)^2} \int\limits_{\mathrm{BZ}} d^2\boldsymbol{k}\, \mathrm{e}^{i\boldsymbol{k}(\boldsymbol{R}-\boldsymbol{R}')} \sum_m \left(\frac{\omega_{m\boldsymbol{k}}}{c}\right)^2 U^*_{mn}(\boldsymbol{k})\, U_{mn'}(\boldsymbol{k}) \,. \tag{22}$$

Due to the smoothness of the photonic dispersion relation $\omega_{n\boldsymbol{k}}$ with respect to the wave vector $\boldsymbol{k}$, the exponential factor in Eq. (22) leads to a very rapid decay of the matrix elements' magnitude with increasing separation $|\boldsymbol{R} - \boldsymbol{R}'|$ between lattice sites, effectively making the matrix $A^{nn'}_{\boldsymbol{R}\boldsymbol{R}'}$ sparse. Furthermore, it may be shown that the matrix $A^{nn'}_{\boldsymbol{R}\boldsymbol{R}'}$ is symmetric and positively definite.

Once the Wannier functions of the underlying PC are determined, the matrix $D^{nn'}_{\boldsymbol{R}\boldsymbol{R}'}$ depends solely on the overlap of these functions which is mediated by the defect structure

$$D^{nn'}_{\boldsymbol{R}\boldsymbol{R}'} = \int\limits_{\mathrm{R}^2} d^2\boldsymbol{r} W^*{}_{n\boldsymbol{R}}(\boldsymbol{r})\, \delta\varepsilon(\boldsymbol{r})\, W_{n'\boldsymbol{R}'}(\boldsymbol{r}) \,. \tag{23}$$

As a consequence of the localization properties of both the Wannier functions and the defect dielectric function, the hermitian matrix $D^{nn'}_{\boldsymbol{R}\boldsymbol{R}'}$, too, is sparse. As an illustration, we consider a cluster of defects by identically modifying four rods in the perfect PC. The positions of the defect rods are shown as black circles in the inset of Fig. 3. Then, the defect dielectric function $\delta\varepsilon(\boldsymbol{r})$ can be written as a sum

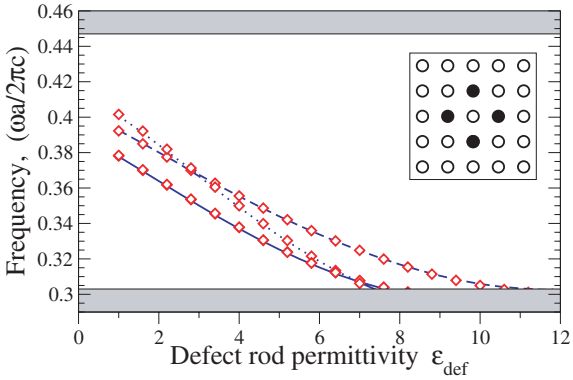

Fig. 3 Frequencies of cavity modes for a cluster consisting of four identical defect rods as a function of the defect dielectric constant $\varepsilon_{\mathrm{def}}$. The position of the defect rods are shown as black circles in the inset. The results of the Wannier function approach ($N_{\mathrm{W}} = 6$, diamonds) are in complete agreement with super-cell calculations for doubly-degenerate dipole cavity modes (solid line), second order monopole cavity mode (dashed line), and quadrupole cavity modes (dotted line). The parameters of the underlying PC are the same as those in Fig 1.

over the corresponding lattice sites $\boldsymbol{S}_i \in \{-\boldsymbol{a}_1, \boldsymbol{a}_1, -\boldsymbol{a}_2, \boldsymbol{a}_2\}$

$$\delta\varepsilon(\boldsymbol{r}) = (\varepsilon_{\mathrm{def}} - \varepsilon_{\mathrm{rod}}) \sum_i \Theta(R_{\mathrm{rod}} - |\boldsymbol{r} - \boldsymbol{S}_i|)\,, \tag{24}$$

where $\Theta(x)$ denotes the Heaviside step function. In Fig. 3, we display the dependence of the cavity frequencies as a function of the defect dielectric constant $\varepsilon_{\mathrm{def}}$. The results of the Wannier function approach using the six energetically lowest lying Wannier functions are fully converged and in complete agreement with the results of corresponding supercell calculations.

To discuss the efficiency of the Wannier function approach, we note that the Wannier function calculations scale linearly with the number of lattice sites and Wannier functions considered. In particular, the present calculations have been carried out within a computational cell containing 7×7 lattice sites. When using the six energetically lowest lying Wannier functions, we obtain a sparse eigenvalue problem, Eq. (21), with a matrix size of 294×294. More importantly, however, is the fact that owing to the translational properties of the Wannier functions, Eq. (17), the computation of the defect clusters requires only the computation of matrix elements for *isolated* defect rods. Therefore, for a given underlying PC structure, it becomes possible to build up a database of matrix elements for different types of isolated defects, which would allow highly efficient defect computations through simple matrix assembly procedures. This is in stark contrast to *any* other computational technique known to us.

Finally, we want to emphasize that the Wannier function approach can be extended to the calculation of PC waveguide dispersion relations as well as transmission and reflection calculations through arbitrary devices [36]. Its efficiency will allow to investigate large-scale PC circuits [36, 37] and facilitates studies of disorder effects in and reverse engineering of such circuits.

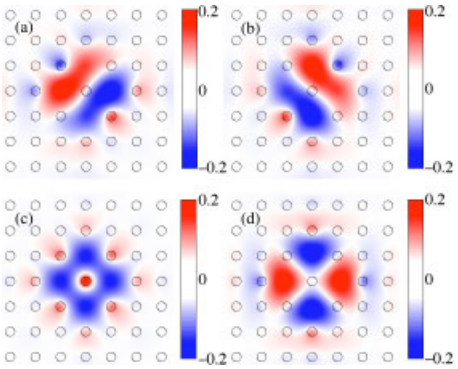

Fig. 4 Localized cavity modes associated with a cluster of defects. Removing four rods from our model PC as depicted in Fig. 3 creates a doubly degenerate dipole mode ($\omega = 0.378 \times 2\pi c/a$, a) and b)), a second-order monopole mode ($\omega = 0.392 \times 2\pi c/a$, c)), and a quadrupole mode ($\omega = 0.402 \times 2\pi c/a$, d)). These results are calculated from Eq. (21) with $N_W = 6$ Wannier functions per unit cell. The parameters of the underlying PC are the same as those in Fig. 1 (see also Fig. 3).

4 Nonlinear photonic crystals

The existence of PBGs and the tailoring of photonic dispersion relations and mode structures through judiciously designed PCs represent a novel paradigm for nonlinear wave interactions. To date, only a few works have been carried out for Kerr-nonlinearities [15–17] or for $\chi^{(2)}$-nonlinearities [23, 38] in PCs. Moreover, the approximations involved seriously limit the applicability of these theories to real PCs. For instance, the study of Kerr-nonlinearities in 2D PCs [15] has been limited to weak modulations in the linear index of refraction. Similarly, the recent investigation of second harmonic generation in 2D PCs [23, 38] failed to reproduce the well-known results for the limiting case of homogeneous materials.

In this section, we outline a systematic approach to quantitative calculations of the optical properties of nonlinear PCs that is based on a multi-scale approach. We start by writing the corresponding wave equation in the time domain and introduce the nonlinear polarization $P_{\mathrm{NL}}(\boldsymbol{r}, t)$, representing the nonlinear response of the system

$$\left(\partial_x^2 + \partial_y^2\right) E(\boldsymbol{r}, t) - \frac{\epsilon_{\mathrm{p}}(\boldsymbol{r})}{c^2}\, \partial_t^2 E(\boldsymbol{r}, t) = \frac{4\pi}{c^2}\, \partial_t^2 P_{\mathrm{NL}}(\boldsymbol{r}, t)\,. \tag{25}$$

Since optical nonlinearities are generally quite weak, Eq. (25) should be solved in a perturbative way taking into account that the effect of the nonlinearity accumulates only on time and spatial scales that are much slower and longer, respectively, than the natural scales of the underlying linear problem. In the case of electromagnetic wave propagation in PCs, these natural scales of the linear problem are determined through the inverse optical period and the associated wavelength of the light. Therefore, key simplifications to Eq. (25) arise from separating the fast from slow scales in space and time in the electromagnetic field $E(\boldsymbol{r}, t)$. This separation is facilitated by formally replacing the space and time variables, $\boldsymbol{r}$ and t, with a set of independent variables $\boldsymbol{r}_n \equiv \mu^n \boldsymbol{r}$ and $t_n \equiv \mu^n t$. For instance, in this multi-scale approach [39] the time derivative is replaced according to

$$\partial_t = \partial_{t_0} + \mu \partial_{t_1} + \mu^2 \partial_{t_2} + \dots\,, \tag{26}$$

and similar replacements of spatial and higher order derivatives. In addition, this is accompanied by a corresponding expansion of the electromagnetic field in powers of the formal expansion parameter μ, in order to construct a hierarchy of equations which effectively separate the different scales of the problem

$$E(\boldsymbol{r}, t) = \mu e_1(\boldsymbol{r}_0, \boldsymbol{r}_1, \dots; t_0, t_1, \dots) + \mu^2 e_2(\boldsymbol{r}_0, \boldsymbol{r}_1, \dots; t_0, t_1, \dots) + \dots\,. \tag{27}$$

Heree, we denote the fastest spatial scale corresponding to the wavelength of the electromagnetic waves propagating in the linear PC by $\boldsymbol{r}_0$. Likewise, we denote the associated fastest temporal scale by t_0. Depending on the type of nonlinearity, the hierarchy is suitably truncated and a closed set of equations is obtained. To express the results in terms of the original physical variables, at the end of the calculations one has to set $\mu = 1$ [28].

As an illustration, we consider the case where at least one of the PC's constituent materials exhibits an intensity dependent index of refraction. For such Kerr-nonlinearities, the nonlinear polarization $P_{\mathrm{NL}}(\boldsymbol{r}, t)$ is given by

$$P_{\mathrm{NL}}(\boldsymbol{r}, t) = \chi^{(3)}(\boldsymbol{r})\, |E(\boldsymbol{r}, t)|^2\, E(\boldsymbol{r}, t)\,. \tag{28}$$

To first order in the expansion parameter μ, i.e., on the fast scale we obtain that the e_1-component of the electromagnetic field obeys Eq. (25) without the nonlinearity. Consequently, we make the ansatz

$$e_1(\boldsymbol{r}_0, \boldsymbol{r}_1, \dots; t_0, t_1, \dots) = a_{n\boldsymbol{k}}(\boldsymbol{r}_1, \dots; t_1, \dots)\, E_{n\boldsymbol{k}}(\boldsymbol{r}_0)\, \mathrm{e}^{i\omega_{n\boldsymbol{k}} t_0}, \tag{29}$$

where the Bloch function $E_{n\boldsymbol{k}}(\boldsymbol{r}_0)$ represents a carrier wave and the envelope function $a_{n\boldsymbol{k}}(\boldsymbol{r}_1, \dots; t_1, \dots)$ has to be determined by explicitly considering the slower scales.

In second order in μ, we obtain that the envelope function a_{nk} is traveling with the group velocity $\boldsymbol{v}_{nk}$ of the carrier wave

$$a_{nk}(\boldsymbol{r}_1, \ldots; t_1, \ldots) \equiv a_{nk}(\boldsymbol{z}_1; \boldsymbol{r}_2 \ldots; t_2, \ldots)\,, \tag{30}$$

where $\boldsymbol{z}_1 \equiv \boldsymbol{r}_1 - \boldsymbol{v}_{nk} t_1$ and the group velocity $\boldsymbol{v}_{nk}$ is given in terms of an expression familiar from $\boldsymbol{k} \cdot \boldsymbol{p}$-perturbation theory Eq. (12).

Finally, in third order in μ, we obtain that the envelope function a_{nk} obeys the 2D nonlinear Schrödinger equation (NLSE)

$$\begin{aligned} &[i(\boldsymbol{v}_{nk} \cdot \nabla_{\boldsymbol{r}_2} + \partial_{t_2}) + \nabla_{\boldsymbol{z}_1} \cdot \mathcal{M}_{nk} \cdot \nabla_{\boldsymbol{z}_1}]\, a_{nk}(\boldsymbol{z}_1; \boldsymbol{r}_2 \ldots; t_2, \ldots) \\ &+ \alpha_{nk}\, |a_{nk}(\boldsymbol{z}_1; \boldsymbol{r}_2 \ldots; t_2, \ldots)|^2\, a_{nk}(\boldsymbol{z}_1; \boldsymbol{r}_2 \ldots; t_2, \ldots) = 0\,, \end{aligned} \tag{31}$$

where the GVD tensor $\mathcal{M}_{nk}$ is given in Eq. (13) and the effective nonlinearity α_{nk} reflects how the carrier wave $E_{nk}(\boldsymbol{r})$ samples the spatial distribution $\chi^{(3)}(\boldsymbol{r})$ of nonlinear material within the PC

$$\alpha_{nk} = 6\pi\, \omega_{nk} \int\limits_{\mathrm{WSC}} \mathrm{d}^2 r\, \chi^{(3)}(\boldsymbol{r})\, |E_{nk}(\boldsymbol{r})|^4\,. \tag{32}$$

The discussion of the solutions to Eq. (31) is outside the scope of the present work and we refer the reader to references on the inverse scattering theory [40]. However, we want to emphasize that, as a result of the foregoing analysis, we have obtained a generalization of the slowly varying envelope approximation. Within this approximation, the problem of pulse propagation in nonlinear PCs is mapped onto the problem of an envelope function propagating in an effective homogeneous medium with group velocity $\boldsymbol{v}_{nk}$, GVD tensor $\mathcal{M}_{nk}$, and effective nonlinearity α_{nk} that are determined by the carrier wave, which, in turn, is given by a Bloch function of the linear PC. Therefore, the effective PC parameters can be obtained from bandstructure theory via Eqs. (12), (13), and (32) and quantitative investigations become possible. Furthermore, we want to note that the above considerations are not limited to 2D TM polarized radiation and have recently been extended to 3D systems by Bhat and Sipe [16]. Moreover, the above framework of multi-scale analysis in conjunction with $\boldsymbol{k} \cdot \boldsymbol{p}$-perturbation theory can be applied to other nonlinear PC systems such as PCs consisting of nonresonant $\chi^{(2)}$ [41] material and resonant distributed feedback lasing systems [25]. In the present case of Kerr nonlinearities, other effects such as nonresonant soliton interactions can be considered and lead to interesting applications [42].

5 Conclusions

In summary, we have outlined a framework based on solid state theoretical methods that allows to qualitatively and quantitatively treat wave propagation in PCs. Photonic bandstructure computation of the infinitely extended PC provides the input necessary to efficiently obtain the properties of defect structures embedded in PCs via expansions into localized Wannier functions and allows the determination of effective parameters such as Densities of States, group velocities, GVD tensors, and effective nonlinearities. In particular, the efficiency of the Wannier function approach to defect structures in PCs allows investigations of PC circuits which, to date, are beyond the reach of standard simulation techniques such as FDTD or finite element methods. In addition, the description of nonlinear PCs through the generalized slowly varying envelope approximation discussed above allows to investigate such systems using a limited number of effective parameters with transparent physical meaning.

Acknowledgments This work was supported by the Center for Functional Nanostructures (CFN) of the Deutsche Forschungsgemeinschaft (DFG) within projects A 1.1, A 1.2, and A 1.3. The research of K.B., A.G.M., and L.T. is further supported by the DFG under grant Bu 1107/2-2 (Emmy-Noether program). M.F. ackowledges the support by the DFG Priority Program SP 1113 *Photonic Crystals*. The work of M.S. is funded in the framework of the DFG Research Training Group 786 *Mixed Fields and Nonlinear Interactions* at the University of Karlsruhe.

References

[1] E. Yablonovitch, Phys. Rev. Lett. **58**, 2059 (1987).
[2] S. John, Phys. Rev. Lett. **58**, 2486 (1987).
[3] Photonic Crystals and Light Localization in the 21st Century, edited by C. M. Soukoulis, NATO Science Series C **563**, (Kluwer Academic, Dordrecht, Boston, London, 2001).
[4] A. Blanco et al., Nature (London) **405**, 437 (2000).
[5] Yu. A. Vlasov et al., Nature (London) **414**, 289 (2001).
[6] S. John and T. Quang, Phys. Rev. A **50**, 1764 (1994).
[7] N. Vats, K. Busch, and S. John, Phys. Rev. A **65**, 043808 (2002).
[8] O. Painter et al., Science **284**, 1819 (1999).
[9] P. L. Philips et al., J. Appl. Phys. **85**, 6337 (1999).
[10] D. Labilloy et al., Phys. Rev. B **59**, 1649 (1999).
[11] U. Grüning, V. Lehmann, and C. M. Engelhardt, Appl. Phys. Lett. **66**, 3254 (1995).
[12] J. Schilling et al., Opt. Mat. **3**, S121 (2001).
[13] S. Fan, P. R. Villeneuve, and H. A. Haus, Phys. Rev. Lett. **80**, 960 (1998).
[14] S. Noda, A. Alongkarn, and M. Imada, Nature (London) **407**, 608 (2000).
[15] N. Aközbek and S. John, Phys. Rev. E **57**, 2287 (1998).
[16] N. Bhat and J. Sipe, Phys. Rev. E **64**, 056604 (2001).
[17] S. F. Mingaleev and Yu. S. Kivshar, Phys. Rev. Lett. **86**, 5474 (2001).
[18] S. F. Mingaleev, Yu. S. Kivshar, and R. A. Sammut, Phys. Rev. E **62**, 5777 (2000).
[19] H. Kosaka, et al., Phys. Rev. B **58**, R10096 (1999).
[20] H. Kosaka, et al., J. Lightwave Technol. **17**, 2032 (1999).
[21] B. Gralak, S. Enoch, and G. Tayeb, J. Opt. Soc. Am. A **17**, 1012 (2000).
[22] M. Notomi, Opt. Quant. Elect. **34**, 133 (2002).
[23] Optical properties of Photonic Crystals, K. Sakoda, (Springer, Berlin, Heidelberg, New York, 2001).
[24] C. Kallinger et al., Adv. Mater. **10**, 920 (1998).
[25] L. Florescu, K. Busch, and S. John, J. Opt. Soc. Am. B **19**, 2215 (2002).
[26] K. Busch and S. John, Phys. Rev. E **58**, 3896 (1998).
[27] K. Busch and S. John, Phys. Rev. Lett. **83**, 967 (1999).
[28] C. Martijn de Sterke and J. E. Sipe, Phys. Rev. A **38**, 5149 (1988).
[29] D. Hermann, M. Frank, K. Busch, and P. Wölfle, Opt. Express **8**, 167 (2001).
[30] J. E. Sipe, Phys. Rev. E **62**, 5672 (2000).
[31] A. Garcia-Martin, D. Hermann, K. Busch, and P. Wölfle, Mat. Res. Symp. Proc. **722**, L1.1 (2002).
[32] A. Garcia-Martin, D. Hermann, F. Hagmann, K. Busch, and P. Wölfle, Nanotechnology **14**, 177 (2003).
[33] N. Marzari and D. Vanderbilt, Phys. Rev. B **56**, 12847 (1997).
[34] I. Souza, N. Marzari, and D. Vanderbilt, Phys. Rev. B **65**, 035109 (2002).
[35] D. M. Whittaker and M. P. Croucher, Phys. Rev. B **67**, 085204 (2003).
[36] K. Busch et al., J. Phys., Condens. Matter, in press.
[37] S. F. Mingaleev and K. Busch, Opt. Lett. **28**, 619 (2003).
[38] K. Sakoda and K. Ohtaka, Phys. Rev. **54**, 5742 (1996).
[39] Perturbation Methods, A. H. Nayfeh, (Wiley, New York, 1973).
[40] Solitons and Nonlinear Wave Equations, R. K. Dodd, J. C. Eilbeck, J. D. Gibbon, and H. C. Morris, (Academic Press, London, 1982).
[41] L. Tkeshelashvili and K. Busch, submitted.
[42] L. Tkeshelashvili, S. Pereira, and K. Busch, submitted.